Electrochemical and Solid-State Letters, **1** (1) 13-16 (1998)
S1099-0062(97)11-069-0 CCC: $7.00

Stabilization of $LiMnO_2$ in the α-$NaFeO_2$ Structure Type by $LiAlO_2$ Addition

Young-Il Jang,* Biying Huang, Yet-Ming Chiang,,‡ and Donald R. Sadoway****

Department of Materials Science and Engineering, Massachusetts Institute of Technology, Cambridge, Massachusetts 02139, USA

$LiMnO_2$ of the α-$NaFeO_2$ structure type has previously been obtained only by the ion-exchange of lithium salts with α-$NaMnO_2$. In this paper, we show that $LiAl_xMn_{1-x}O_2$ solid solutions can be crystallized in this structure under conditions where neither pure end-member does. The compounds were synthesized by firing homogeneous hydroxide precursors in a reducing atmosphere to control the manganese valence state. A composition $LiAl_{0.25}Mn_{0.75}O_2$ shows a first-charging voltage of ~4 V against a lithium electrode, but develops 4 and 3 V plateaus upon cycling, indicating transformation to spinel-like cation ordering within the oxide. Unlike previously reported lithium manganese spinels, the compound of this study shows excellent reversible capacity (148 mAh/g at C/5 rate; 182 mAh/g at C/15 rate) when cycled over both the 4 and 3 V plateaus, and an energy density (545 Wh/kg) surpassing that of the spinels.
 S1099-0062(97)11-069-0

Manuscript submitted November 21, 1997; revised manuscript received February 18, 1998.

$LiMnO_2$ compounds have come to be of interest as intercalation electrodes for rechargeable lithium batteries because of their high theoretical capacity (285 mAh/g), about twice that of $LiMn_2O_4$, and low cost relative to $LiCoO_2$. Orthorhombic $LiMnO_2$ (hereafter referred to as *o*-$LiMnO_2$) has been known since 1956[1] and has an ordered rock salt structure of space group *Pmnm*.[2] It is now well known that *o*-$LiMnO_2$ transforms irreversibly to a material with spinel-like ordering upon electrochemical cycling.[3-9] Another phase of interest in this system is the monoclinic polymorph of $LiMnO_2$ (hereafter referred to as *m*-$LiMnO_2$), which has the cation ordering of the α-$NaFeO_2$ structure, in which Li^+ ions are located in octahedral sites between MnO_6 sheets. Unlike $LiCoO_2$, which is rhombohedral (*R3m*), $LiMnO_2$ is monoclinic (*C2/m*) because the coordination polyhedron around the Mn^{3+} ions is distorted from a regular octahedron due to the Jahn-Teller effect.[10] Recently, *m*-$LiMnO_2$ has been obtained by an ion-exchange reaction of LiCl and LiBr with α-$NaMnO_2$.[10-12] As with *o*-$LiMnO_2$, this material appears to convert from its original layered α-$NaFeO_2$ structure to a spinel-like structure during cycling, based on X-ray diffraction after electrochemical cycling and the appearance of both 4 and 3 V plateaus in the charge/discharge curves.[12]

$LiMn_2O_4$ shows significant capacity fade when cycled over both the 4 and 3 V plateaus.[3,13] The onset of the Jahn-Teller distortion and the consequent structural instability when $Li_xMn_2O_4$ is discharged to an average manganese valence < 3.5 (i.e., at $x \geq 1$) is generally believed to contribute to the rapid capacity loss.[14,15] Even when $LiMn_2O_4$ is cycled over only the 4 V plateau, a slow capacity fade is usually observed.[16-18] Some efforts have been made, as reviewed in Ref. 19, to extend the capacity to include the 3 V plateau without significantly deteriorating the cycling behavior.

Both *o*- and *m*-$LiMnO_2$ have shown better cycleability than $LiMn_2O_4$ when both the 4 and 3 V plateaus are utilized.[3-6,8,9,12] The reversible capacity reported to date for long-term cycling remains much less than the theoretical capacity. For example, 45-200 mAh/g has been obtained from *o*-$LiMnO_2$ between 2.5 and 4.3 V depending on the synthesis condition and charge/discharge rate.[8,9] The materials of higher capacity also appear to fade more rapidly upon cycling.[9] In *m*-$LiMnO_2$, ~110 mAh/g has been obtained between 2.0 and 4.5 V.[12] A greater fraction of the theoretical capacity may be achievable with appropriate modifications of these phases.

Although doped $LiMn_2O_4$ spinels have been studied,[20-25] to our knowledge the stabilization of *o*- or *m*-$LiMnO_2$ by doping has not been reported. We chose to study $LiAl_xMn_{1-x}O_2$ solid solutions for several reasons. Ab initio calculations by Aydinol et al.[26] have shown that $LiAlO_2$ has a theoretical intercalation voltage of 5.4 V (against lithium metal anode). While pure $LiAlO_2$ is electrochemically inactive, the solid solution of $LiAlO_2$ with various lithiated transition-metal oxides can potentially increase the intercalation voltage and cathode energy density.[27] This effect has recently been confirmed for $Li_xAl_yCo_{1-y}O_2$ solid solutions.[27] $Li_xAl_yMn_{1-y}O_2$ solid solutions are of interest as another test of these voltage mixing rules. Second, the fact that $LiAlO_2$ is stable in the α-$NaFeO_2$ structure at temperatures below ~600°C[28] suggests that it could have a stabilizing effect on $LiMnO_2$. Finally, its low cost and low density make $LiAlO_2$ attractive as a constituent of intercalation electrodes.

Experimental

$LiOH{\bullet}H_2O$ (Alfa Aesar, 98%), $Mn(NO_3)_3{\bullet}6H_2O$ (Aldrich, 98%), and $Al(NO_3)_3(9H_2O$ (Alfa Aesar, 98%) were used to prepare the precursors. Precursors with and without aluminum doping were prepared by the same method. Precursors (A) were aluminum-doped at the levels y=0.05 and y=0.25, and had a Li:(Mn+Al) atomic ratio of 1.05:1. The slight excess of Li was included to compensate for loss during firing. Precursor (B) was undoped with a Li:Mn atomic ratio of 1.05:1. For precursors (A), a mixed manganese-aluminum hydroxide was coprecipitated from mixed aqueous solutions of $Mn(NO_3)_3{\bullet}6H_2O$ and $Al(NO_3)_3{\bullet}9H_2O$. The precipitate was purified of nitrate ion species, which otherwise re-form low-melting metal nitrates upon firing, by a rinsing procedure described in Ref. 29. The precipitate was then dispersed in an aqueous solution of $LiOH{\bullet}H_2O$ yielding the total compositions given above. This suspension was atomized into liquid nitrogen, and the frozen droplets were freeze-dried (VirTis Consol 12LL, Gardiner, NY). Precursor (B) was obtained by the same method but using $Mn(NO_3)_3{\bullet}6H_2O$ alone. A more detailed description of this synthesis method can be found in Ref. 29.

The precursor powders were fired for 2 h at 945°C in various partial pressures of oxygen and furnace-cooled to room temperature. $LiMn_2O_4$ and Li_2MnO_3 are the phases usually obtained when oxides with Li/Mn ~1 are fired in air.[30,31] A reducing atmosphere was used in order to obtain a high Mn^{3+} fraction. The effect of oxygen partial pressure on the phase stability was studied by firing in the range $po_2 = 10^{-2}$ to 10^{-7} atm, controlled by flowing premixed argon/oxygen or CO/CO_2 mixtures. The calcined powders were characterized by X-ray diffraction (XRD) using a Rigaku diffractometer (RTP500RC) with Cu K_α radiation.

For electrochemical evaluation, cathodes were prepared by mixing together the oxide powders, carbon black (Cabot), graphite (TIMCAL America), and poly(vinylidene fluoride) (PVDF, Aldrich) in the weight ratio of 78:6:6:10. PVDF was predissolved in γ-butyrolacetone (Aldrich) before mixing with the other components. After the γ-butyrolactone was evaporated at 150°C in air, the components were compacted at about 4 t/cm^2 pressure to form pellets 10-25 mg in weight and 0.5 cm^2 in cross-sectional area. The pellets were then dried at 140°C under primary vacuum for 24 h and transferred into an argon-filled glove box.

* Electrochemical Society Student Member.
** Electrochemical Society Active Member.
‡ E-mail: YCHIANG@MIT.EDU

S1099-0062(97)11-069-0 CCC: $7.00

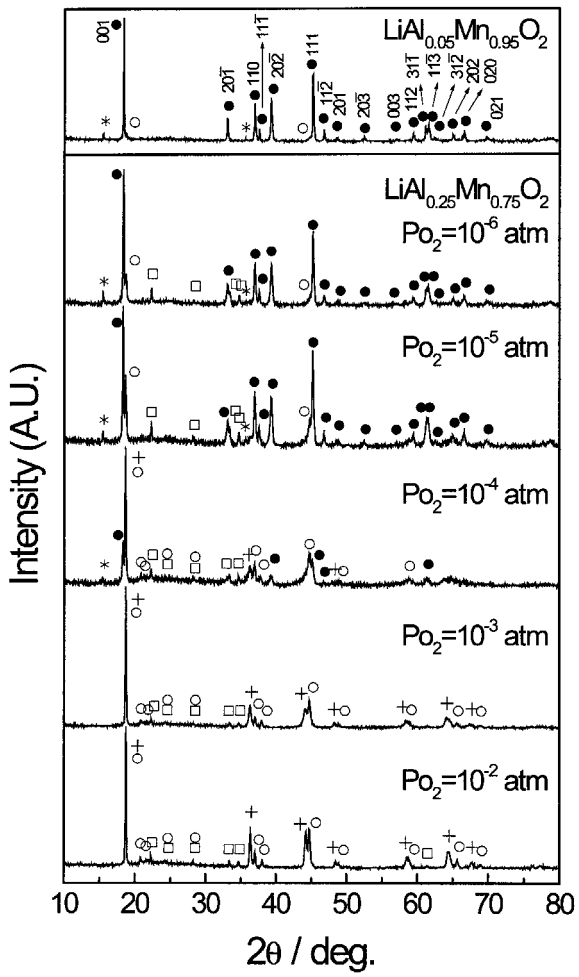

Figure 1. Powder XRD patterns of $LiAl_yMn_{1-y}O_2$ after firing for 2 h at 945°C in various oxygen partial pressures. (●: *m*-$LiMnO_2$, with *hkl* indicated; ∗: *o*-$LiMnO_2$; +: $LiMn_2O_4$; ❍: Li_2MnO_3; and ❑: γ-$LiAlO_2$). The top pattern for $LiAl_{0.05}Mn_{0.95}O_2$ corresponds to $P_{O_2}=10^{-7}$ atm firing conditions.

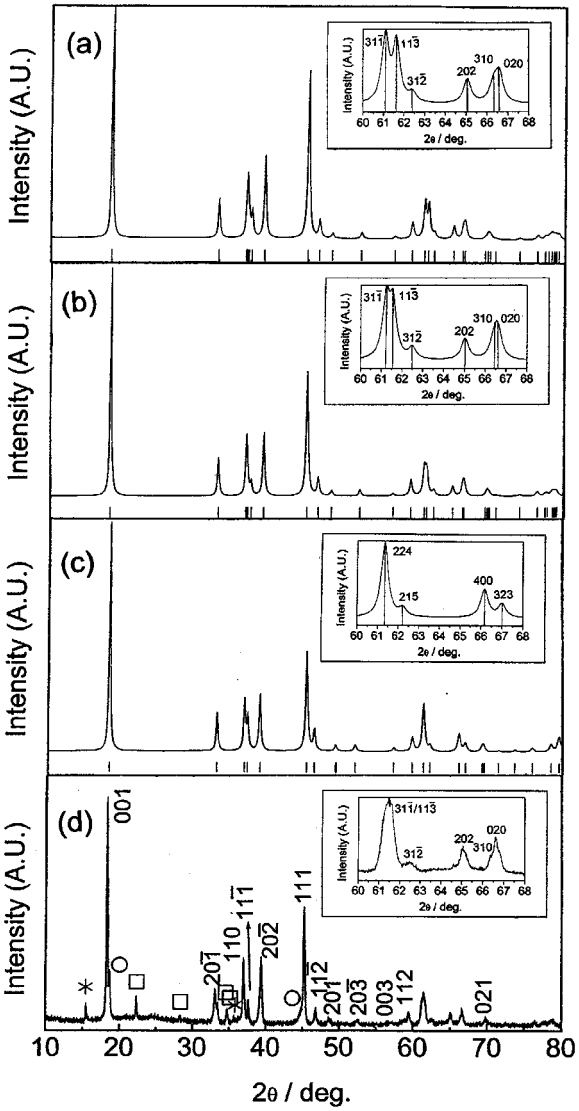

Figure 2. Simulated XRD patterns for (a) *m*-$LiMnO_2$, (b) *m*-$LiAl_{0.25}Mn_{0.75}O_2$, and (c) $Li_2Mn_2O_4$, compared with (d) the experimental pattern for $LiAl_{0.25}Mn_{0.75}O_2$.

The electrochemical test cell consisted of two stainless steel electrodes with a Teflon holder. Lithium ribbon of 0.75 mm thickness (Aldrich) was used as the negative electrode (anode). The separator was a film of Celgard 2400™ (Hoechst-Celanese, Charlotte, NC), and the electrolyte consisted of a 1 M solution of $LiPF_6$ in ethylene carbonate (EC) and diethyl carbonate (DEC). The ratio of EC to DEC was 1:1 by volume. All cell handling was performed in an argon-filled glove box. Charge-discharge studies were performed with a MACCOR automated test equipment (series 4000). Data were taken at a constant current density of 0.40 or 0.133 mA/cm^2, corresponding to a rate of C/5 or C/15, between 2.0 and 4.4 V at room temperature.

Results and Discussion

XRD patterns of the oxide powders obtained by firing the aluminum-doped precursors at 945°C in various oxygen partial pressures are shown in Fig. 1. At the higher oxygen partial pressures of 10^{-2} and 10^{-3} atm, the resulting phases are $LiMn_2O_4$, Li_2MnO_3, and γ-$LiAlO_2$ (tetragonal phase). As the oxygen partial pressure is reduced further, however, new phases begin to form. At 10^{-4} atm, these new phases are sufficiently distinct to be identifiable as being isostructural with *m*-$LiMnO_2$ and *o*-$LiMnO_2$. *m*-$LiMnO_2$, marked by its strongest peak at 2θ = 18.3°, becomes the major phase at oxygen partial pressures below 10^{-5} atm. The identification of this phase is discussed in greater detail below. The amount of *o*-$LiMnO_2$ also increases slightly as the oxygen partial pressure decreases between 10^{-4} and 10^{-6} atm, but it remains a minor phase throughout. The more lightly aluminum doped sample of composition $LiAl_{0.05}Mn_{0.95}O_2$ exhibited exclusively the *m*-$LiMnO_2$ phase when fired in reducing atmosphere ($P_{O_2}=10^{-7}$ atm, Fig. 1). The XRD results indicate that the predominant manganese valence state is 3+ at oxygen partial pressures below 10^{-4} atm. Under these conditions, a solid solution between the $LiAlO_2$ and $LiMnO_2$ end members is achieved.

It should be noted that the XRD pattern of *m*-$LiMnO_2$ is very similar to that of tetragonal $Li_2Mn_2O_4$ spinel, which has been obtained by lithiation of $LiMn_2O_4$ spinel.[13] Capitaine et al.[11] have argued that these two phases can be distinguished from each other by the diffraction lines in the 64-68° 2θ range. For a more detailed examination, we simulated the XRD patterns of *m*-$LiMnO_2$, $Li_2Mn_2O_4$, and a hypothetical solid solution *m*-$LiAl_{0.25}Mn_{0.75}O_2$, using the commercial software Cerius^2 (v.3.5, Molecular Simulations Inc., San Diego, CA). The structure of *m*-$LiMnO_2$ was simulated using crystallographic data from Armstrong and Bruce,[10] that for $Li_2Mn_2O_4$ using data from Mosbah et al.,[32] and that for *m*-$LiAl_{0.25}Mn_{0.75}O_2$ using the lattice parameters determined in this study (see below) and the Armstrong and Bruce oxygen parameters, assuming completely ordered α-$NaFeO_2$ structure except for the substitution of 25% of the Mn by Al.

The simulated results are shown in Fig. 2 in comparison with the experimental XRD pattern for $LiAl_{0.25}Mn_{0.75}O_2$. Clear differences between the three simulated patterns can be seen in the positions and relative intensities of peaks in the 60-68° range, expanded in the inset for each pattern. The monoclinic phases, *m*-$LiMnO_2$ and *m*-

S1099-0062(97)11-069-0 CCC: $7.00 © The Electrochemical Society, Inc.

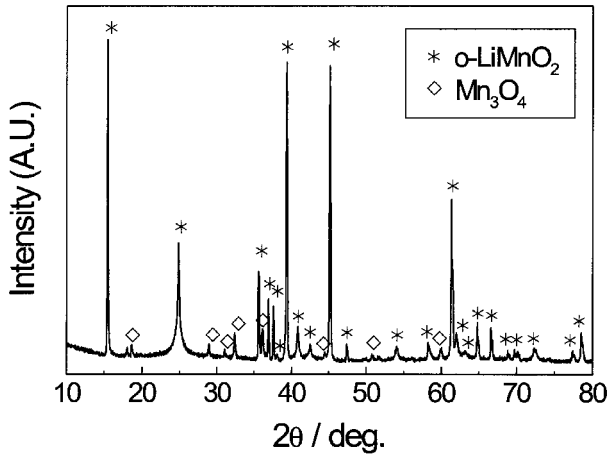

Figure 3. Powder XRD pattern of undoped precursor after firing for 2 h at 945°C and Po_2=10^{-6} atm (❊: *o*-$LiMnO_2$; ✧: Mn_3O_4)

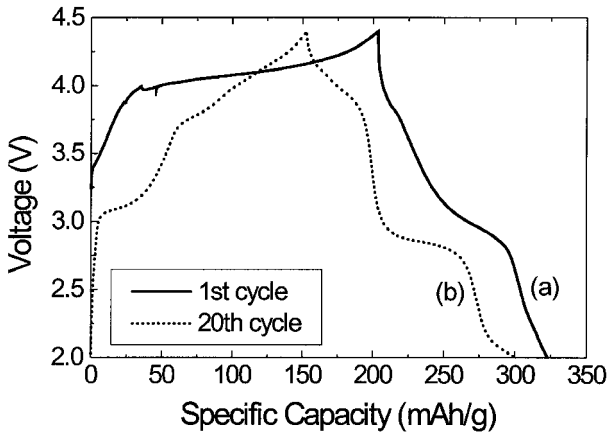

Figure 4. (a) First charge-discharge curve for *m*-$LiAl_{0.25}Mn_{0.75}O_2$, tested against a lithium metal anode in a cell at 0.4 mA/cm_2 current density (C/5 rate) between 2.0 and 4.4 V. (b) Charge-discharge curve for the cell in (a) after 20 cycles at 0.4 mA/cm^2 current density (C/5 rate) between 2.0 and 4.4 V.

$LiAl_{0.25}Mn_{0.75}O_2$, exhibit (202) and (020) peaks at 65.1 and 66.6°, respectively, with the latter being of higher intensity. $Li_2Mn_2O_4$ has (400) and (323) peaks at 66.1 and 67.0°, respectively, with the former being of higher intensity. The experimental pattern in Fig. 2(d) exhibits peak positions (65.1 and 66.6°) as well as relative intensities that correspond to the monoclinic phase. According to our results, the statement by Capitaine et al.[11] that *m*-$LiMnO_2$ has two peaks in the 64-68° 2θ range while $Li_2Mn_2O_4$ has only one is not quite correct.

Another distinguishable feature between the different phases is observed in the range 61-62°. *m*-$LiMnO_2$ has two peaks ($3\bar{1}1$) and ($11\bar{3}$), which become more closely spaced in *m*-$LiAl_{0.25}Mn_{0.75}O_2$. $Li_2Mn_2O_4$ has only one peak (224) in this 2θ range. The experimental pattern (Fig. 2d) matches the simulation for *m*-$LiAl_{0.25}Mn_{0.75}O_2$ better than that for *m*-$LiMnO_2$. Taken together, the XRD results strongly support the identification of the present phase as being of the monoclinic structure, and having Al substituted for Mn. Direct observation and energy-dispersive X-ray mapping of the oxide powder particles with scanning transmission electron microscopy has also confirmed that the Al and Mn are uniformly distributed throughout the particles.

As further support, undoped $Li_2Mn_2O_4$ is known to be unstable under the temperature and atmosphere conditions of this study, transforming to *o*-$LiMnO_2$.[13] Figure 3 shows the XRD pattern of the undoped $LiMnO_2$ sample obtained by firing precursor (B) at 945°C in 10^{-6} atm oxygen partial pressure. *o*-$LiMnO_2$ is indeed seen to be the predominant phase, consistent with the reported stability of this phase under these conditions.[13]

Table I. Monoclinic unit cell parameters of the present *m*-$LiAl_{0.25}Mn_{0.75}O_2$ in comparison with those of pure *m*-$LiMnO_2$ obtained by ion-exchange reaction.

	m-$LiA_{l0.25}Mn_{0.75}O_2$ (This study)	*m*-$LiMnO_2$ (Ref. 10)	*m*-$LiMnO_2$ (Ref. 11)	*m*-$LiMnO_2$ (Ref. 12)
a	5.426 ± 0.003Å	5.4387(7) Å	5.439(3) Å	5.431(6) Å
b	2.806 ± 0.001Å	2.80857(4) Å	2.809(2) Å	2.809(2) Å
c	5.384 ± 0.003Å	5.3878(6) Å	5.395(4) Å	5.390 Å
β	115.96 ± 0.03°	116.006(3)°	115.9(4)°	115.95(7)°

It is therefore clear that the stabilization of *m*-$LiAl_yMn_{1-y}O_2$ phase is due to the addition of aluminum and not to the firing conditions alone. We also note that the α-$NaFeO_2$ polymorph of $LiAlO_2$ (α-$LiAlO_2$) is not the stable phase under these conditions; it is known to irreversibly transform to γ-$LiAlO_2$ above 600°C.[28] The present $LiAl_xMn_{1-x}O_2$ solid solution is therefore seen to crystallize in the α-$NaFeO_2$ cation ordering under conditions where neither end member, $LiAlO_2$ nor $LiMnO_2$, is stable in this structure.

The lattice parameters of the *m*-$LiAl_{0.25}Mn_{0.75}O_2$ have been calculated from the XRD data using Cohen's least-squares method, and are compared with those for pure *m*-$LiMnO_2$ obtained by the ion-exchange method in Table I. Within the precision of the data, no significant differences are found in the values of *b* and β, while *a* and *c* are slightly decreased.

Figure 4 shows the first charge-discharge curve (C/5 rate) of a cell prepared using the *m*-$LiAl_{0.25}Mn_{0.75}O_2$ (fired at 945°C, P_{O_2} = 10^{-6} atm) as the cathode and lithium metal as the anode. It can be seen that the cell exhibits a single charging voltage plateau at ~4 V, and has about 203 mAh/g of first-charge capacity. A similar result has been reported for the first charging cycle of pure *m*-$LiMnO_2$ by Vitins and West.[12] There does not appear to be a significant difference in average voltage between pure *m*-$LiMnO_2$ and *m*-$LiAl_{0.25}Mn_{0.75}O_2$, although the comparison may not be exact since the materials are prepared and tested under different conditions. In addition, this sample is not purely single phase (Fig. 1), and the aluminum concentration in the monoclinic phase may be somewhat less than the nominal composition. Furthermore, evidence for a change in cation order during cycling (see below) indicates that the observed potential may include the energetics of other simultaneous processes. In Li(Al,Co)O_2, an increase of the average voltage by ~0.15 V has been observed at this aluminum doping level.[27] More-detailed studies are necessary to understand if the voltage mixing rules are indeed different in these two systems.

The first-discharge curve shows a capacity of about 119 mAh/g and the emergence of two voltage steps. After further cycling, the voltage steps become more distinct. Figure 4 also shows the charge-discharge curve at the 20th cycle, where two plateaus at ~4 and ~3 V are clearly seen, indicating intercalation at two distinct lithium sites. This behavior is characteristic of the spinel phase $Li_xMn_2O_4$, in which lithium is inserted into the tetrahedral sites over the 4 V plateau corresponding to $0< x \leq 1$, while lithium is inserted into the octahedral sites over the 3 V plateau corresponding to $1\leq x \leq 2$.[33] It can be concluded that the present *m*-$LiAl_{0.25}Mn_{0.75}O_2$, which initially has only octahedral cation occupancy, has transformed upon cycling to a material with at least a local spinel-like cation ordering. Taking these results and previous observations together,[3-9,12] it is clear that both the monoclinic and orthorhombic polymorphs of $LiMnO_2$ have a strong tendency to transform to a spinel-like cation ordering during electrochemical cycling.

Figure 5 shows the evolution of the charge and discharge capacities during cycling between 2.0 and 4.4 V at C/5 rate. While an initial drop in capacity to about 100 mAh/g is seen over the first 5 cycles, with further cycling the discharge capacity increases progressively, and saturates after about 15 cycles at ~148 mAh/g. The initial decrease in capacity is likely related to existence of an intermediate stage of cation ordering. The fact that cycling can be conducted over both the 4 and 3 V plateaus without capacity fade is a remarkably different behavior from that of $LiMn_2O_4$ spinel, in which the capacity decreases rapidly

S1099-0062(97)11-069-0 CCC: $7.00

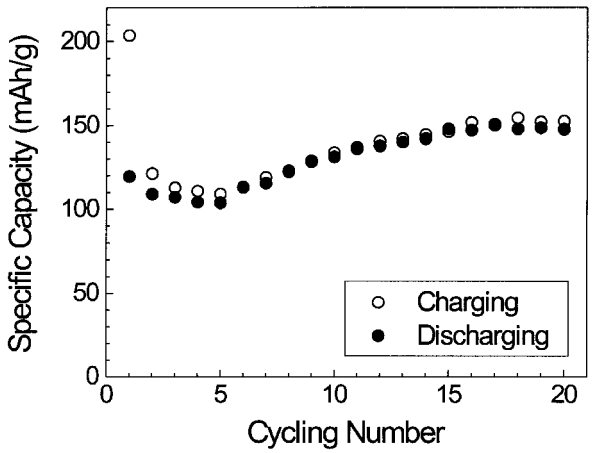

Figure 5. Specific capacity vs. cycle number for *m*-$LiAl_{0.25}Mn_{0.75}O_2$, tested against a lithium metal anode at 0.4 mA/cm^2 current density (C/5 rate) between 2.0 and 4.4 V.

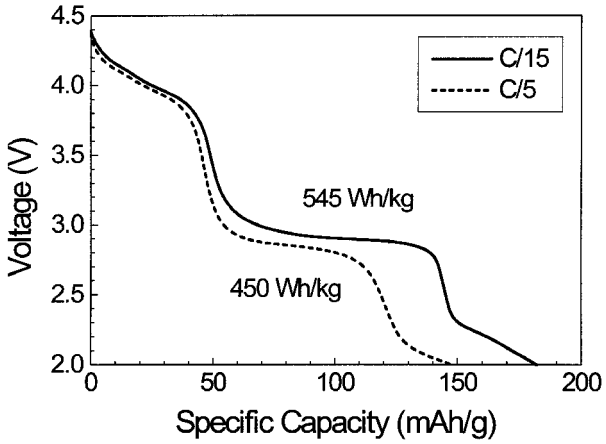

Figure 6. Discharge curves for *m*-$LiAl_{0.25}Mn_{0.75}O_2$ at C/5 and C/15 rates. The C/5 curve is the 20th discharge after cycling between 2.0 and 4.4 V. The C/15 curve represents an accelerated cycling experiment in which the sample was first cycled 12 times at C/5 rate between 2.0 and 4.4 V, and the 13th cycle (shown) was conducted at C/15 rate. The corresponding energy densities are shown.

upon cycling into the 3 V region. A similar resistance to capacity fade has been seen in *o*-$LiMnO_2$ prepared under certain conditions.[8,9] In both cases, the Mn^{3+} fraction is high, yet the Jahn-Teller distortion to which capacity fade is attributed in the spinels seems not to have a serious effect.

Because reversible capacities and energy densities are often strongly dependent on the charge/discharge rate, we did limited tests of the *m*-$LiAl_{0.25}Mn_{0.75}O_2$ material at a lower C/15 rate. To accelerate any cycling fade, the sample was first cycled 12 times at C/5 rate. The 13th cycle at C/15 rate is shown in Fig. 6 in comparison with the result at C/5 rate. It is seen that the reversible capacity increases to 182 mAh/g at the lower rate, with an energy density of 545 Wh/kg. At the C/5 rate, the energy density is 450 Wh/kg.

Comparisons with the capacities and energy densities reported for $LiCoO_2$, $LiMn_2O_4$, and *o*-$LiMnO_2$ shows that the present material has promise for practical application in lithium-ion batteries. Generally, the reversible capacities of $LiCoO_2$ and $LiMn_2O_4$ fall in the range 120-130 mAh/g, with energy densities in the range 480-520 Wh/kg.[19] Croguennec et al. reported capacities as high as 200 mAh/g for *o*-$LiMnO_2$ at a C/15 charge-discharge rate utilizing both the 4 and 3 V plateaus, with some capacity fade.[8,9] Materials which exhibited less fade apparently had lower capacities (<140 mAh/g).[9] The theoretical capacity of *m*-$LiAl_{0.25}Mn_{0.75}O_2$ is 231 mAh/g if it is assumed that lithium ions can be reversibly extracted until the average manganese valence is 4+. Our measured capacity is ~64 % of this theoretical value at C/5 rate and 78% at C/15 rate. Further improvements may be possible in $LiAl_xMn_{1-x}O_2$ solid solutions with additional study.

Conclusions

A $LiAl_xMn_{1-x}O_2$ solid solution can be crystallized in the monoclinic derivative of the α-$NaFeO_2$ structure upon firing in a reducing environment to control the Mn^{3+} content. During electrochemical cycling, this compound develops two voltage plateaus (4 and 3 V, vs. a lithium anode), suggesting spinel-like cation ordering, as previously observed for *o*-$LiMnO_2$ and *m*-$LiMnO_2$ prepared by other methods. However, the resulting material shows excellent cycleability and high reversible capacity when cycled over both voltage plateaus, unlike the $LiMn_2O_4$ spinels. A composition $LiAl_{0.25}Mn_{0.75}O_2$ exhibited 148 mAh/g reversible capacity at C/5 rate (450 Wh/kg energy density) and 182 mAh/g at C/15 rate (545 Wh/kg). *m*-$LiAl_xMn_{1-x}O_2$ solid solutions may therefore be attractive cathode materials for low-cost, high-energy-density lithium rechargeable batteries.

Acknowledgments

We thank G. Ceder and A. M. Mayes for helpful discussions, and H. Wang for experimental assistance. This project has been funded by Furukawa Electric Co., Ltd., and by the INEEL University Research Consortium. The INEEL is managed by Lockheed Martin Idaho Technology Company for the U.S. DOE, Idaho Operations Offices, under contract no. DE-AC07-94ID13223. We used instrumentation in the Shared Central Facilities at MIT, supported by NSF grant no. 9400334-DMR.

MIT assisted in meeting the publication costs of this article.

References

1. W. D. Johnston and R. R. Heikes, *J. Am. Chem. Soc.*, **78**, 3255 (1956).
2. R. Hoppe, G. Brachtel, and M. Jansen, *Z. Anorg. Allg. Chem.*, **417**, 1 (1975).
3. R. J. Gummow and M. M. Thackeray, *J. Electrochem. Soc.*, **141**, 1178 (1994).
4. J. N. Reimers, E. W. Fuller, E. Rossen, and J. R. Dahn, *J. Electrochem. Soc.*, **140**, 3396 (1993).
5. R. J. Gummow, D. C. Liles, and M. M. Thackeray, *Mater. Res. Bull.*, **28**, 1249 (1993).
6. I. J. Davidson, R. J. McMillan, J. J. Murray, and J. E. Greedan, *J. Power Sources*, **54**, 232 (1995).
7. I. Koetschau, M. N. Richard, J. R. Dahn, J. B. Soupart, and J. C. Rousche, *J. Electrochem. Soc.*, **142**, 2906 (1995).
8. L. Croguennec, P. Deniard, R. Brec, P. Biensan, and M. Broussely, *Solid State Ionics*, **89**, 127 (1996).
9. L. Croguennec, P. Deniard, and R. Brec, *J. Electrochem. Soc.*, **144**, 3323 (1997).
10. A. R. Armstrong and P. G. Bruce, *Nature*, **381**, 499 (1996).
11. F. Capitaine, P. Gravereau, and C. Delmas, *Solid State Ionics*, **89**, 197 (1996).
12. G. Vitins and K. West, *J. Electrochem. Soc.*, **144**, 2587 (1997).
13. J. M. Tarascon and D. Guyomard, *J. Electrochem. Soc.*, **138**, 2864 (1991).
14. M. M. Thackeray, A. de Kock, M. H. Rossouw, D. Liles, R. Bittihn, and D. Hoge, *J. Electrochem. Soc.*, **139**, 363 (1992).
15. J. Barker, R. Koksbang, and M. Y. Saïdi, *Solid State Ionics*, **82**, 143 (1995).
16. R. J. Gummow, A. de Kock, and M. M. Thackeray, *Solid State Ionics*, **69**, 59 (1994).
17. D. H. Jang, Y. J. Shin, and S. M. Oh, *J. Electrochem. Soc.*, **143**, 2204 (1996).
18. Y. Xia, Y. Zhou, and M. Yoshio, *J. Electrochem. Soc.*, **144**, 2593 (1997).
19. R. Koksbang, J. Barker, H. Shi, and M. Y. Saïdi, *Solid State Ionics*, **84**, 1 (1996).
20. J. M. Tarascon, E. Wang, F. K. Shokoohi, W. R. McKinnon, and S. Colson, *J. Electrochem. Soc.*, **138**, 2859 (1991).
21. C. Sigala, D. Guyomard, A. Verbaere, Y. Piffard, and M. Tournoux, *Solid State Ionics*, **81**, 167 (1995).
22. L. Guohua, H. Ikuta, T. Uchida, and M. Wakihara, *J. Electrochem. Soc.*, **143**, 178 (1996).
23. K. Amine, H. Tukamoto, H. Yasuda, and Y. Fujita, *J. Electrochem. Soc.*, **143**, 1607 (1997).
24. F. Le Cras, D. Bloch, M. Anne, and P. Strobel, *Solid State Ionics*, **89**, 203 (1996).
25. Q. Zhong, A. Bonakdarpour, M. Zhang, Y. Gao, and J. R. Dahn, *J. Electrochem. Soc.*, **144**, 205 (1997).
26. M. K. Aydinol, A. F. Kohan, G. Ceder, K. Cho, and J. Joannopoulos, *Phys. Rev. B*, **56**, 1354 (1997).
27. G. Ceder, Y.-M. Chiang, D. R. Sadoway, M. K. Aydinol, Y.-I. Jang, and B. Huang, *Nature*, **392**, 694 (1998).
28. H. A. Lehmann and H. Hesselbarth, *Z. Anorg. Allg. Chem.*, **313**, 117 (1961).
29. Y.-M. Chiang, Y.-I. Jang, H. Wang, B. Huang, D. R. Sadoway, and P. Ye, *J. Electrochem. Soc.*, **145**, 887 (1998).
30. M. H. Rossouw, A. de Kock, L. A. de Picciotto, and M. M. Thackeray, *Mater. Res. Bull.*, **25**, 173 (1990).
31. V. Massarotti, D. Capsoni, M. Bini, C. B. Azzoni, and A. Paleari, *J. Solid State Chem.*, **128**, 80 (1997).
32. A. Mosbah, A. Verbaere, and M. Tournoux, *Mater. Res. Bull.*, **18**, 1375 (1983).
33. M. M. Thackeray, W. I. F. David, P. G. Bruce, and J. B. Goodenough, *Mat. Res. Bull.*, **18**, 461 (1983).